Int. J. Electrochem. Sci., 13 **(2018)** 4753 – 4762, doi: 10.20964/2018.05.22

International Journal of
ELECTROCHEMICAL
SCIENCE
www.electrochemsci.org

Template Synthesis of Highly Dispersed $LiNi_{0.5}Mn_{1.5}O_4$ Thin Flakes with Improved Electrochemical Performance using Filter Paper

Hongyan Sun[1,2], Xin Kong[1,2], Baosen Wang[1,2], Tingbi Luo[1,2], Ying He[1,2],Guiyang Liu[1,2,]*

[1] Department of Chemistry, College of Science, Honghe University, Mengzi, 661199, Yunnan, China
[2] Local Characteristic Resource Utilization and New Materials Key Laboratory of Universities in Yunnan, Honghe University, Mengzi 661199, Yunnan, China.
[*]E-mail: liuguiyang@tsinghua.org.cn

Received: 26 December 2017 / *Accepted:* 23 February 2018 / *Published:* 10 April 2018

A highly dispersed flaky $LiNi_{0.5}Mn_{1.5}O_4$ has been successfully prepared using one-step filter paper assisted templated method. The phase structures of the products were investigated by X-ray powder diffraction (XRD) and infrared spectroscopy (FT-IR) techniques. The micro morphologies of the products were observed by scanning electron microscopy (SEM). The electrochemical performances were studied by galvanostatic charge-discharge testing, cyclic voltammetry(CV) and electrochemical impedance spectroscopy (EIS). The results show that both of the $LiNi_{0.5}Mn_{1.5}O_4$ prepared by filter paper assisted templated method (LNMO-FP) and the non-templated $LiNi_{0.5}Mn_{1.5}O_4$ (LNMO) exhibit a high degree of ordered space group. The LNMO-FP shows a thin flake micro morphology, which consists of highly dispersed and well crystallined grains. In contrast, the LNMO sample dispays a badly agglomerate morphology. Moreover, the electrochemical performances of the LNMO-FP are obviously improved compared with the LNMO including both cycling stability and rate capability. It is because that the LNMO-FP sample has higher crystallinity, larger diffusion coefficients of Li^+ and lower polarization.

Keywords: Lithium ion battery; $LiNi_{0.5}Mn_{1.5}O_4$; template-assisted method; filter paper

1. INTRODUCTION

Rechargeable lithium ion batteries are considered as promising energy storage devices for electronic devices as well as electric vehicles(EV) and hybrid electric vehicles(HEV) due to their high energy density, high power density, superior safety, long cycle life, and so on[1,2]. The spinel $LiNi_{0.5}Mn_{1.5}O_4$ has been regarded as a particularly attractive cathode material for lithium ion batteries because of its high operating voltage, high specific energy, fast Li^+ diffusion within the three-

dimensional spinel lattices, low cost as well as good cycling performance and environment-friendliness [3-5]. However, the performances of $LiNi_{0.5}Mn_{1.5}O_4$ need to be further improved substantially especially rate capability in order to meet the more demanding requirements of these large energy storage systems of EVs and HEVs. It is because that lithium ion batteries need to work at large current densities, for example fast charging and fast discharging [6]. It has been proved that electrode materials with nanostructure and good dispersivity have excellent rate performances[7-9]. $LiNi_{0.5}Mn_{1.5}O_4$ materials possessing nanostructures such as nanoplates, nanofibers and nanorods have been reported as excellent materials with good rate performance. Yang's group[10] successfully synthesized $LiNi_{0.5}Mn_{1.5}O_4$ nanoplates using two-step technique including a hydrothermal method and a solid-state reaction. The as-prepared LNMO nanoplates delivered a high specific discharge capacity of 134mAh/g at 15C rate and 120.9mAh/g at 40C rate, respectively. It is because that the nanoplate structure can shorten the diffusion path of Li^+ and promote the fast charge-discharge properties. Arun's group [11] prepared $LiNi_{0.5}Mn_{1.5}O_4$ nanofibers via a spinneret electro-spinning method. The cycling performance and rate capability had been markedly improved. The capacity retention was about 86% for initial reversible capacity with an operating potential of 2.8V. $LiNi_{0.5}Mn_{1.5}O_4$ porous nanorods were prepared via morphology-inheritance route reported by Zhang's group[9]. The porous nanorods of $LiNi_{0.5}Mn_{1.5}O_4$ exhibited specific capacities of 140 mAh/g at 1C and 109 mAh/g and 20C. The capacity retention of 91% was sustained after 500 cycles at 5C. In our previous studies, porous $LiNi_{0.5}Mn_{1.5}O_4$ materials were synthesized by one step templated method using corn stalk or pine wood as bio-templates and they both displayed significant improved performance including cycling stability, rate capacity and specific capacity compared with the non-templated products [12,13].

In this paper, filter paper was used as a new template to synthesize $LiNi_{0.5}Mn_{1.5}O_4$. As the template, filter paper could be easily removed during the high-temperature calcination, and no additional processing was needed. Because of the limitation of the filter paper during the formation of the materials, the as-prepared $LiNi_{0.5}Mn_{1.5}O_4$ shows a thin flake micro morphology. The grains of the product are small and highly dispersed. It means that the product can obtain good rate capability. Hereinafter the electrochemical performances of the products would be investigated in details.

2. EXPERIMENTAL

2.1 Synthesis

The raw materials of $LiNO_3$, CH_3COOLi, $Ni(NO_3)_2$, $(CH_3COO)_2Ni$, $Mn(NO_3)_2$ and $(CH_3COO)_2Mn$ with the mole ratio of 0.5:0.5:0.25:0.25:0.75:0.75 were dissolved in proper distilled water to form uniform green solution with a metal concentration of 3mol/L. The filter papers working as template were firstly cut to small tablets and dried. Then the filter paper tablets were immersed into above mentioned solution for 10min and then taken out. And then, the filter paper with soaking solution was first dried at 150^{o}C for 2h and then calcined at 700 ^{o}C for 12h in a muffle furnace. The product was cooled down to room temperature in the furnace and marked as LNMO-FP. The treatment processes above all were conducted in air atmosphere. The samples were marked as LNMO obtained from the raw materials solution directly, which treated at the same conditions for comparison.

2.2 Characterization

Powder X-ray diffraction (XRD, PANalytical X'pert pro, Cu-Kα radiation) and Fourier transformed infrared spectroscopy(FT-IR, PerkinElmer, with KBr pellets) were used to characterize the structures of the LNMO-FP and LNMO samples. Field emission scanning electron microscopy (SEM, FEI Quanta FEG 250) was employed to observe the morphologies of the samples.

2.3 Electrochemical performance test

The electrochemical properties were characterized by using CR2032-type coin cells which were assembled in a high purity argon-filled glove box. The cathode electrodes contained about 80wt.% active material, 10wt.% carbon black and 10wt.% polyvinylidene difluoride(PVDF). The anode electrode is Li metal foil. Porous Celgard 2400 polyethylene membrane was used to as the separator. The electrolyte was 1M LiPF6 in a mixed solution of ethylene carbonate(EC) and dimethyl carbonate(DEC) with a weight ratio of 1:1.

The cells were galvanostatically charged and discharged at different discharge rates (0.5C, 1C, 2C, 5C and 10C) with a voltage range from 3.5V to 5.0V. And here, 1C=150mA/g. Cyclic voltammogram(CV) measurements were performed using an electrochemical workstation(CHI 660) at different scan rates from 0.1 to 0.3mV/s. And the voltages of galvanostatically charged and discharged were between 3.5V and 5.0V. Electrochemical impedance spectroscopy (EIS) tests were measured using the CHI 660 type electrochemical workstation. The frequency range was from 0.1Hz to 100 kHz and the amplitude of ac voltage was 5mV. Except for high temperature tests, all the other tests were conducted at room temperature.

3. RESULTS AND DISCUSSION

3.1 Phase structure

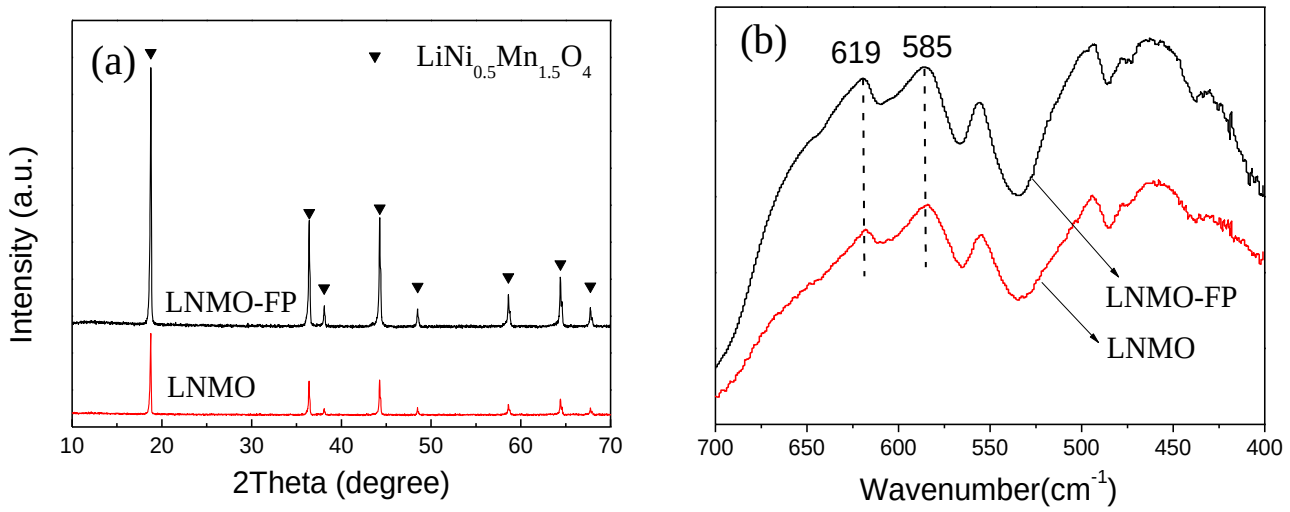

Figure 1. (a) XRD patterns and (b) FT-IR spectra of LNMO-FP and LNMO

Fig. 1(a) shows the XRD patterns of LNMO-FP and LNMO samples. As shown, the results display that the samples are both pure well-defined cubic spinels. And no traces of impurity phases were observed. In the both products, there are two type phase structures of $LiNi_{0.5}Mn_{1.5}O_4$ spinel, ordered $P4_332$ and disordered Fd-3m, which also were reported by other researchers [14,15]. However, XRD is difficult to distinguish the structure ordering of the $LiNi_{0.5}Mn_{1.5}O_4$ material. FT-IR spectroscopy has been reported to be an effective method, which was used to differentiate the ordered versus disordered structures of LNMO cathodes[16-18]. The FT-IR spectra of LNMO-FP and LNMO products are shown in Fig. 1(b). As seen in Fig. 1(b), the intensity of Mn-O band at 619 cm^{-1} is much lower than that of Ni-O band at 585 cm^{-1}, indicating that the LNMO-FP and LNMO samples mostly consists of ordered ($P4_332$) phase with a very small amount of disordered(Fd-3m) phase[19,20].

3.2 Morphology

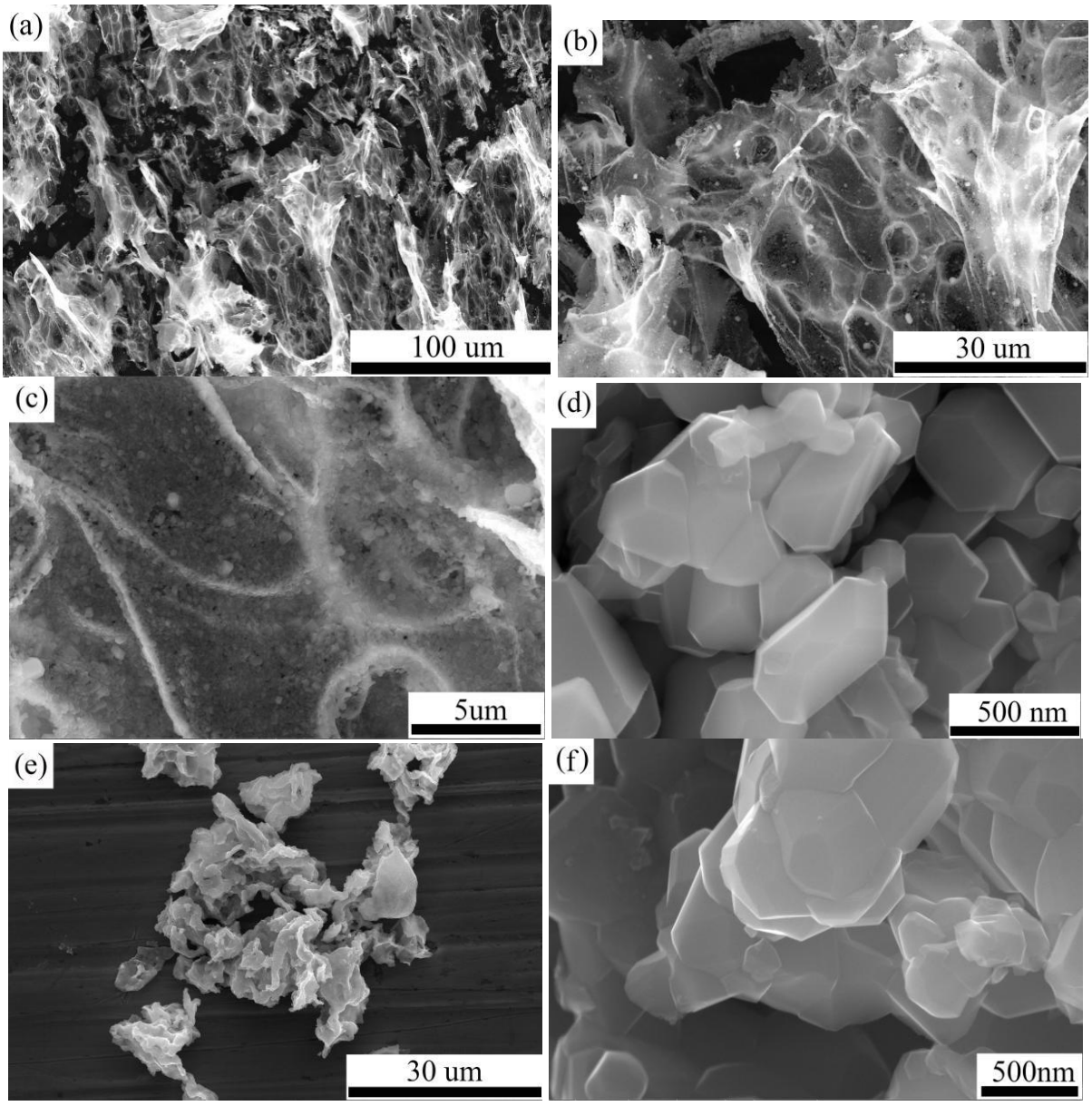

Figure. 2 SEM(a-d) images of LNMO-FP, and SEM(e and f) images of LNMO

Fig. 2 gives the SEM micrographs of LNMO-FP(a-d) and LNMO(e and f). Apparently, the LNMO-FP sample exhibits thin flake-like aspect. It can be seen from the high magnifying power SEM image that the flake is composed of highly dispersed grains. The grains show typical spinel octahedral aspect, indicating that the product is well crystallined. In contrast, the LNMO sample displays agglomerated bulk morphologies and the grain growth is imperfect.

3.3 Electrochemical performance

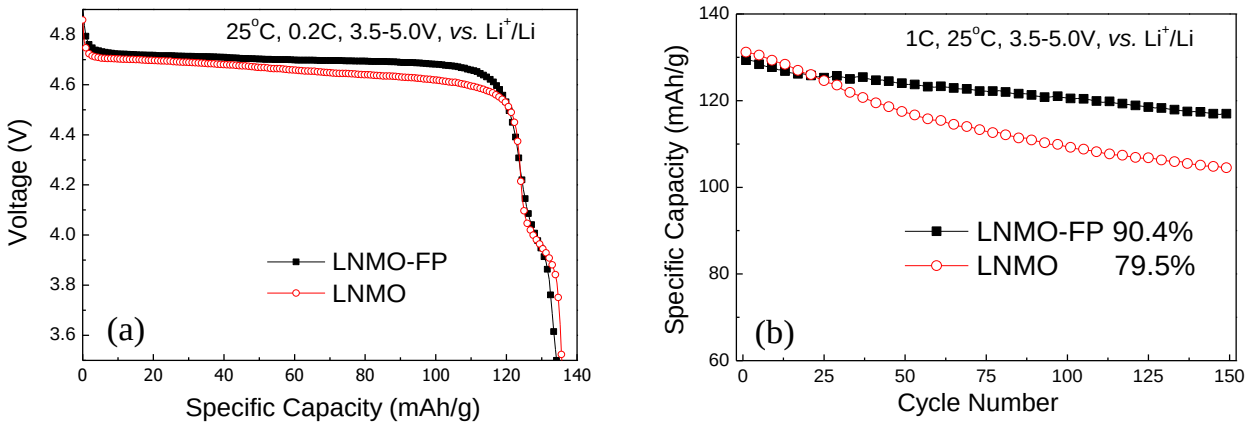

Figure 3. (a) Initial discharge curves for LNMO-FP and LNMO and (b) Cycling performance of LNMO-FP and LNMO at 1C and at 25℃

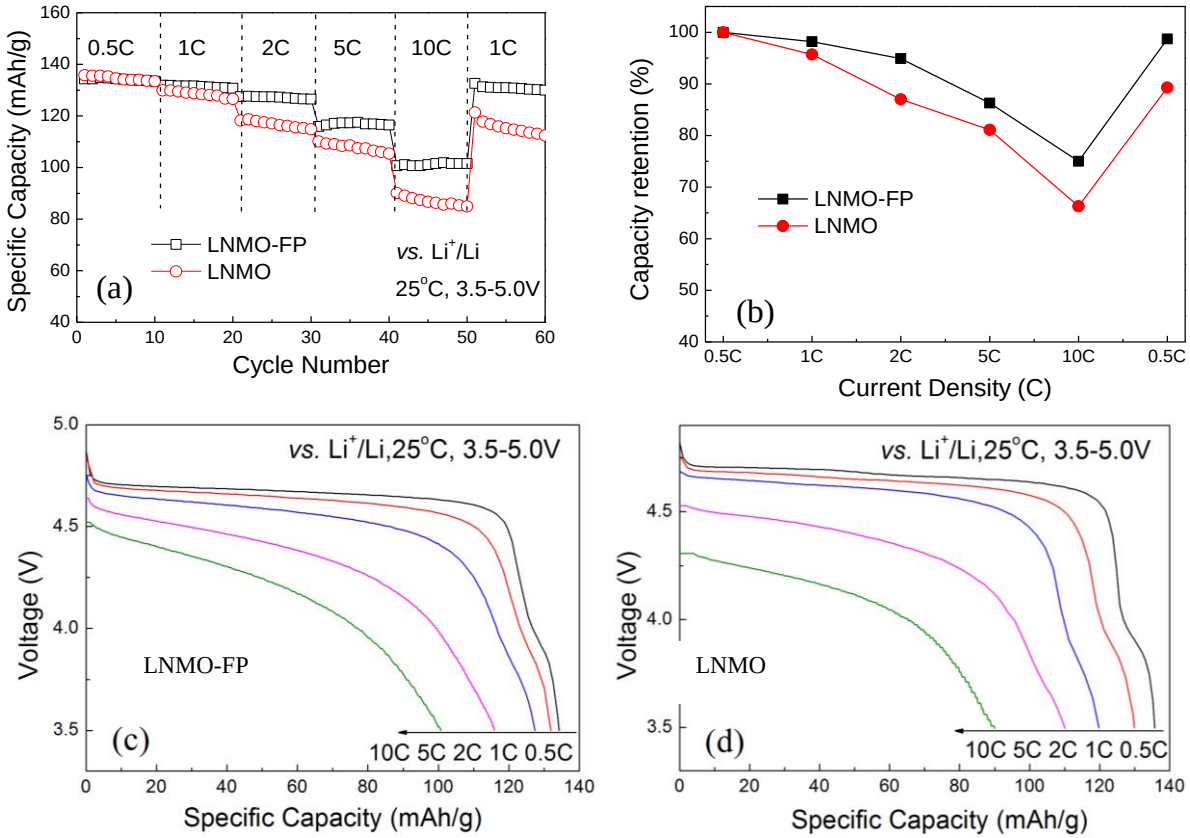

Figure 4. (a)The rate capabilities, (b) capacity retentions, (c and d) discharge profiles at various C rates of LNMO-FP and LNMO at 25℃

The initial discharge curve and cycling performance of LNMO-FP and LNMO samples at 1C rate and at room temperature are given in Fig. 3. From Fig. 3(a), it shows that the initial discharge specific capacities of LNMO-FP and LNMO are 134mAh/g and 136mAh/g, respectively. The 4.7V potential plateau of LNMO-FP is higher than that of LNMO, indicating that the LNMO-FP sample has a smaller polarization. At the same time, the potential plateaus at 4.0V of LNMO-FP and LNMO are both small, revealing that both of the samples have high degree of structure ordering, which is accordance with the FT-IR results above. The same conclusions were also found by Y.C. Jin [21]. Fig. 3(b) contrasts the cycling stability of LNMO-FP and LNMO samples. The LNMO-FP sample delivers the remarkable capacity retention of 90.4% after 150 cycles, while the pristine LNMO sample delivers a capacity retention of only 79.5%. This indicates that the cycling performance is significantly improved by the LNMO-FP sample. Compared with $LiNi_{0.5}Mn_{1.5}O_4$ prepared by the thermopolymerization method[22] and the improved solid-state method[23], the cycle stability of the LNMO-FP is also superior. The comparison of the cycle performance at room temperature is summarized in Table 1.

Table 1. Comparison of the cycle performance at room temperature

Literatures	Samples	The capacity retention/%	Testing conditions
Our research	LNMO-FP	90.4	1C, 150th cycle
Reference[22]	$LiNi_{0.5}Mn_{1.5}O_4$	89.23	1C, 100th cycle
Reference[23]	$LiNi_{0.5}Mn_{1.5}O_4$	81.33	0.2C, 100th cycle

In Fig. 4(a), the rate capabilities of LNMO-FP and LNMO samples are compared. The samples were charged at 0.5C and discharged at different C rates of 0.5C, 1C, 2C, 5C and 10C, and then back to 1C. As shown, the capacities of the two samples decrease with the increase of discharge rate because of electrode polarization. However, the decreasing trend has been obviously reduced in the LNMO-FP sample. Fig. 4(b) shows the capacity retentions of LNMO-FP and LNMO samples at different rates compared with the capacity at 0.5C, which is taken as 100%. It is evident that the rate capability of LNMO-FP is better. The possible reason is that LNMO-FP has a highly dispersed flake-like structure with abundant porous structure and high active surface area, which is benefit for the diffusion of the Li^+ ions in the electrodes[24]. The galvanostatic discharge profiles of LNMO-FP and LNMO samples at different rates are provided in Fig. 4(c and d). With the increasing of rate, the LNMO sample shows a bigger voltage drop and a bigger capacity decrease than these of the LNMO-FP sample. At 10C, the operating discharge voltage of LNMO is lower than 4.3V and the capacity is only about 90 mAh/g. But the LNMO-FP spinels demonstrate a higher discharge voltage of 4.5V and much higher capacity of about 100mAh/g at the rate of 10C. The rate performance of LNMO-FP is also superior to many other $LiNi_{0.5}Mn_{1.5}O_4$ and porous materials reported previously [24-26]. The comparison of the discharge capacity at high rate is displayed in Table 2.

Table 2. Comparison of the Discharge Capacity at High Rate

Literatures	Samples	The discharge capacity/(mAh/g)	Testing conditions
Our research	LNMO-FP	110	10C
Reference[24]	Porous $LiMn_2O_4$	90	10C
Reference[25]	5% Na-LNMO	101	10C
Reference[26]	$LiMn_{1.45}Cr_{0.1}Ni_{0.45}O_4$	40	5C

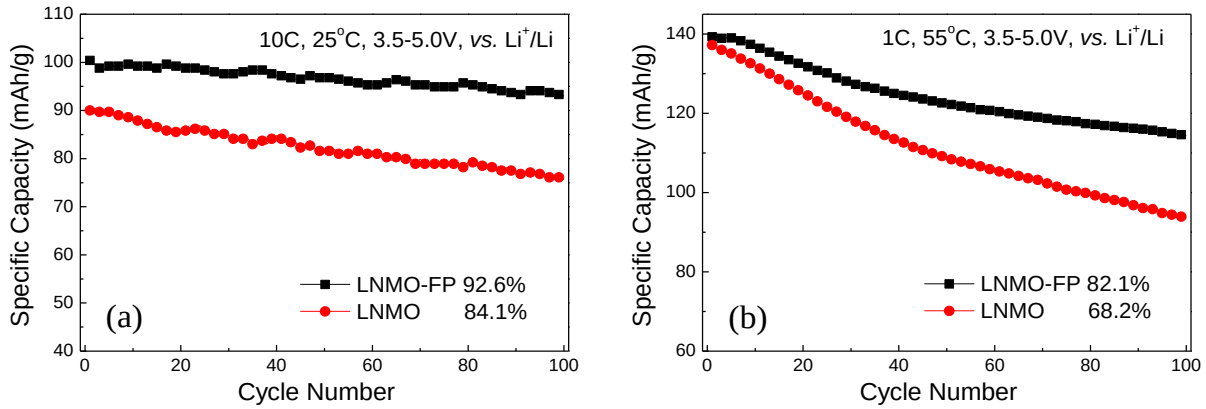

Figure 5. (a) Cycling performance of LNMO-FP and LNMO at 10C and at 25℃ and (b) at 1C and at 55℃

The cycling performance at high rate and at elevated temperature is both significant considering parameters for lithium ion batteries in practical application. Fig. 5(a) shows the cycling stability of the LNMO-FP and LNMO samples at 10C discharge rate (charged at 0.5C). From Fig. 5(a), it is notable that the LNMO-FP sample delivers capacity retention of 92.6% after 100 cycles, exhibiting the excellent cycle performance at high rate. In contrast, the LNMO sample exhibits poor cycle stability at high rate, which can only retain 84.1% of the initial discharge capacity. Fig. 5(b) displays the cycling stability of LNMO-FP and LNMO at 55°C at 1C. In Fig. 5(b), the LNMO-FP displays a significant improved cycling performance at 55°C. The capacity retention of the LNMO-FP sample is still up to 82.1% after 100 cycles at 55 °C. However, the capacity of the LNMO sample decreases rapidly and only retains 68.2% after 100 cycles at the same temperature.

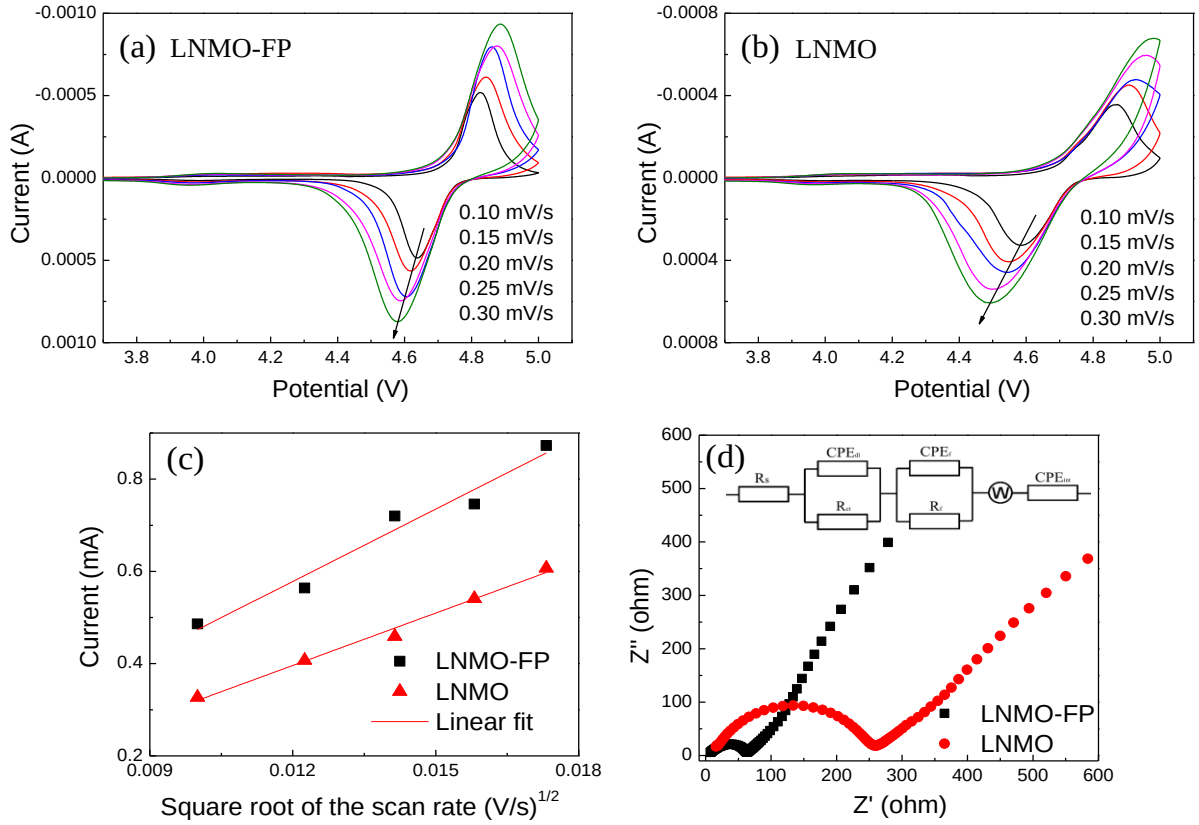

Figure 6. (a and b) Cyclic voltammograms of LNMO-FP and LNMO at different scan rates from 0.10mV/s to 0.30mV/s, (c) the plotting of peak current vs. square root of the scan rate for LNMO-FP and LNMO samples and (d) EIS spectra of LNMO-FP and LNMO samples in the frequency range from 0.1Hz to 100kHz

In order to better interpret the reason for the excellent electrochemical performance of the LNMO-FP samples, the cyclic voltammograms(CV) tests are performed. Fig. 6(a) and Fig. 6(b) show the CV curves of the two samples at the scanning rate from 0.10mV/s to 0.30mV/s. The two samples both possess a sharp oxidation/reduction peak of Ni^{2+}/Ni^{4+} around 4.7 and a very small oxidation/reduction peak of Mn^{3+}/Mn^{4+} around 4.0V, indicating that the two samples both have high degree of structural ordering. Meanwhile, the peak position and shape changes of LNMO-FP are very small with increasing scanning rate, suggesting that the sample has a low polarization. It is reported that the CV test technique can be used to study the diffusion coefficients of Li^+(D_{Li}) in solid LNMO electrodes [27]. It shows a positive proportional relationship between CV peak current and the square root of the sweep rate. And D_{Li} can be calculated from Equation(1) at room temperature.

$$i_p = 2.69\times10^5 n^{\frac{3}{2}} A C_{Li} D_{Li}^{\frac{1}{2}} \upsilon^{\frac{1}{2}} \quad \text{(Eq.1)}$$

In where, I_p is the peak current(A), n is the number of electrons per reaction species (for lithium-ion, n=1), A is the electrode area (2 cm^2 in this study) and C_{Li} is the bulk concentration of Li^+ in the electrode (given as 0.02378 mol/cm^3) [28].

The i_p vs. the square root of the scan rates ($v^{1/2}$) of the LNMO-FP and LNMO samples are presented in Fig. 6(c). D_{Li} can be calculated for the slop of I_p vs $v^{1/2}$ plots according to Eq.1. The D_{Li} of the LNMO-FP electrode and the LNMO electrode are 1.67 × $10^{-11}$$cm^2/s$ and 8.75 × $10^{-12}$$cm^2/s$,

respectively. The D_{Li} value of the LNMO-FP sample is about twice that of the LNMO sample. It is a possible reason that the LNMO-FP has better rate capability than the LNMO.

Fig. 6(d) compares the EIS spectra of the two samples at open-circuit voltage. The EIS spectra exhibit the same profile composed by a depressed semicircle and an inclined line at high-to-middle frequency part and at low frequency part, respectively. The intercept at the Z' axis is the electrolyte resistance (R_s). The semicircle assigns to the charge transfer resistance (R_{ct}) and the lithium-ion migration resistance (R_f) through the multilayer surface films. And its value can be determined from the diameter of the semicircle[29,30]. From Fig. 6(d) we can see that, the R_{ct} and R_f of the LNMO-FP sample are much smaller than those of the LNMO sample, suggesting that the LNMO-FP has faster lithium insertion/extraction kinetics than the LNMO. It is another possible reason that the LNMO-FP has better rate capability than the LNMO.

4. CONCLUSIONS

In the work, a highly dispersed flaky $LiNi_{0.5}Mn_{1.5}O_4$ has been successfully synthesized using a one-step filter paper assisted templated method. The LNMO-FP sample shows better cycling stability, better rate capability at high rate and better cycle performance at elevated temperature than those of the LNMO sample. The capacity retention of the LNMO-FP sample is up to 90.4% after 150 cycles at room temperature at 1C rate, while the capacity retention of the LNMO sample is only 79.5%. Even at 10C rate, the specific capacity of LNMO-FP is about 100mAh/g and can retain 92.6% after 100 cycles, while the specific capacity and the capacity retention of LNMO at 10C are only 90mAh/g and 84.1%, respectively. Moreover, the capacity retention of the LNMO-FP sample is over 82.1% at 55℃ after 100 cycles, but the LNMO product is only 68.2% at the same condition.

ACKNOWLEDGEMENT
The authors gratefully acknowledge the financial supports from the National Natural Science Foundation of China(No. 51362012, No. 51662007 and U1602273), the Key Construction Disciplines of Chemistry for Master Degree Program in Yunnan and Yunnan Applied Basic Research Project (No.2017FD157).

References

1. D.W. Shin, C.A. Bridges, A. Huq, M.P. Paranthaman and A. Manthiram, *Chem. Mater.*, 24 (2012) 3720.
2. E.S. Lee, K.W. Nam, E. Hu and A. Manthiram, *Chem. Mater*., 24 (2012) 3610.
3. T.F. Yi, Y.M. Li, Xi.Y. Li, J.J. Pan, Q.Y. Zhang and Y.R. Zhu, *Sci. Bull*., 62 (2017) 1004.
4. Y. Luo, H.Y. Li, T.L. Lu, Y.X. Zhang, S.S. Mao, Z. Liu, W. Wen, J.Y. Xie and L.Q. Yan, *Electrochim. Acta,* 238 (2017) 237.
5. W. Wu, J.L. Guo, X. Qin, C.B. Bi, J.F. Wang, L. Wang and G.C. Liang, *J. Alloys Compd.*, 721 (2017) 721.
6. J. M. Tarascon and M. Armand, *Nature*, 2001, 414 (6861) 359.
7. X.Y. Zhou, G.H. Chen, J.J. Tang, Y.P. Ren and J. Yang, *J. Power Sources*, 299 (2015) 97.
8. N. Arun, A. Jain, V. Aravindan, S. Jayaraman, W.C. Ling, M.P. Srinivasan and S. Madhavi, *Nano Energy,* 12 (2015) 69.

9. X.L. Zhang, F.Y. Cheng, J.G. Yang and J. Chen, *Nano Lett.*, 13 (2013) 2822.
10. S.F. Yang, J. Chen, Y.J. Liu and B.L. Yi, *J. Mater. Chem.*, A 2 (2014) 9322.
11. N. Arun, V. Aravindan, S. Jayaraman, N. Shubha, W.C. Ling, S. Ramakrishna and S. Madhavi, *Nanoscale*, 6 (2014) 8926.
12. G.Y. Liu, X. Kong, H.Y. Sun, B.S. Wang, Z.Z. Yi and Q.B. Wang, *Electrochim. Acta*, 141 (2014) 141.
13. G.Y. Liu, Y.N. Li and B.S. Wang, *Mater. Lett.*, 139 (2015) 385.
14. T.F. Yi, J. Mei and Y.R. Zhu, *J. Power Sources*, 316 (2016) 85.
15. M. Hu, X.L. Pang and Z. Zhou, *J. Power Sources*, 237 (2013) 229.
16. T.F. Yi, Y.R. Zhu, *Electrochim. Acta* 53 (2008) 3210.
17. N. Amdouni, K. Zaghib, F. Gendron, A. Mauger and C.M. Julien, *Ionics*, 12 (2006) 117.
18. G.Z. Ma, Y. Zhang, J.T. Lin, Z.J. Chen, R.R. Zhao, L.Y. Zou and H.Y. Chen, *J. Solid State Electrochem.*, 11 (2015) 3365.
19. G.B. Zhong, Y.Y. Wang, Z.C. Zhang and C.H. Chen, *Electrochim. Acta*, 56 (2011) 6554.
20. H.Y. Sun, X. Kong, B.S. Wang, T.B. Luo and G.Y. Liu, *Int. J. Electrochem. Sci*., 12 (2017) 8609.
21. Y.C. Jin, C.Y. Lin, J.G. Duh, *Electrochim. Acta* 69 (2012) 45.
22. G.B. Zhong, Y.Y. Wang, Z.C. Zhang and C.H. Chen, *Electrochim. Acta*, 56 (2011) 6554.
23. X.Y. Feng, C. Shen, H.F. Xiang, H.K. Liu, Y.C. Wu and C.H. Chen, *J. Alloys Compd.*, 695 (2017) 227.
24. Y.Z. Wang, X. Shao, H.Y. Xu, M. Xie, S.X. Deng, H. Wang, J.B. Liu and H. Yan, *J. Power Sources*, 226 (2013) 140.
25. J. Wang, W.Q. Lin, B.H. Wu and J.B. Zhao, *Electrochim. Acta*, 145 (2014) 245.
26. D. Liu, J.H. Paquet, J. Trottier, F. Barray, V. Gariépy, P. Hovington, A. Guerfi, A. Mauger, M. Julien, J.B. Goodenough and K. Zaghib, *J. Power Sources*, 217 (2012) 400.
27. F. Lantelme and E. Cherrat, *J. Electroanal. Chem. Interfacial Electrochem.*, 244 (1988) 61.
28. J.L.Wang, Z.H. Li, J. Yang, J.J. Tang, J.J. Yu, W.B. Nie, G.T. Lei and Q.Z. Xiao, *Electrochim. Acta*, 75 (2012) 115.
29. X.L. Li, W. Guo, Y.F. Liu, W.X. He and Z.H. Xiao, *Electrochim. Acta*, 116 (2014) 278.
30. J. Liu and A. Manthiram, *Chem. Mater.*, 21 (2009) 1695.